

# DESIGN OF THE COMPRESSION SYSTEM OF A GEARED TURBOFAN

Thomas Immery, Markus Schnoes, Maximilian Vieweg and Eberhard Nicke

Institute of Propulsion Technology  
German Aerospace Center (DLR)  
Linder Hoehe, 51147 Koeln, Germany  
e-mail: thomas.immery@dlr.de

## ABSTRACT

The geared turbofan aircraft engine is an efficient type of aircraft engine. By using a gearbox, the fan can run at a different rotational speed in comparison to the shaft connecting low pressure compressor and turbine. To assess the in-house tools for preliminary design, a geared turbofan, with the same requirements as the Pratt&Whitney 1000G, is designed, including thermodynamic cycle, turbine, compressor, burner and structural mechanics.

The goal of this study is the design of the compression system, composed of the low-pressure compressor, the inter-compressor duct and the high-pressure compressor. The following steps have been carried out to design the compression system: first, a preliminary design of both compressors is realized, following by a detailed design, conducted with throughflow calculations and the use of a database of optimal airfoils<sup>[1]</sup>. Three stages have been chosen for the low-pressure compressor and eight stages for the high-pressure compressor. In order to reach the target conditions for all operating points from the specifications, the schedule for the variable guide vanes has also been decided on. The final design is validated with 3D CFD calculations. Additionally, the interaction of the inter-compressor duct with the low-pressure and the high-pressure compressor is investigated.

## NOMENCLATURE

ACDC	Advanced Compressor Design Code
ADP	Aerodynamic Design Point
CFD	Computational Fluid Dynamics
HPC	High Pressure Compressor
ICD	Inter Compressor Duct
IGV	Inlet Guide Vane
MCT	Maximum Continuous Thrust
MVDR	Meridional Velocity Density Ratio
OGV	Outlet Guide Vane
TOC	Top of Climb
TOS	Top of Sideline
VGW	Variable Guide Vane
$y^+$	$y^+ = \frac{\rho \times u_\tau \times y}{\mu}$ Non-dimensional distance of the first grid node of the wall
$\alpha$	Duct turning angle
$\gamma$	Blade stagger angle
$\Delta R$	Difference between the mean radius at the inlet of the inter-compressor duct and the mean radius at the outlet of the inter-compressor duct
L	Length of the inter-compressor duct

## INTRODUCTION

The demand for a cost-effective transport system and the careful use of resources and the environment are currently posing major challenges for aviation. To be able to meet the increasing demands in the future, the improvement of existing technologies as well as the use of new technologies, especially in the area of engines, is unavoidable. In addition to the design and the detailed consideration of individual engine components, their integration into the overall system as well as the understanding of existing interactions is essential for a successful conception of engines which meet future requirements.

In the framework of the project PERFECT, the design of a geared turbofan, with the same requirements as the Pratt&Whitney 1100G, is conducted. One of the core tasks of this project is to improve the connection of component design and overall system analysis.

The objectives of this study are, on one hand, to improve and validate the design methodology in the department and, on the other hand, to quantify the results obtained with the in-house tools, such as the streamline curvature program "ACDC", compared to

the results obtained with the in-house 3D CFD simulation software "TRACE".

This paper will only describe the design of the compression system of this engine. This article begins by introducing the characteristics of the main parts of the compression system chosen during the preliminary design. Afterward, the design methods used to design the low-pressure compressor, also called Booster, the high-pressure compressor (HPC) and the inter-compressor duct (ICD) are explained. Additionally, a quick explanation of the blading design method from [1] [5] is presented. Finally, 3D CFD calculations, used to validate the designs obtained with throughflow calculations, are depicted.

## 1. PRELIMINARY DESIGN

The compression system is composed of three parts : the low-pressure compressor, the inter-compressor duct and the high-pressure compressor. Three stages have been chosen for the low-pressure compressor and eight stages for the high-pressure compressor.

The cruise point has been chosen to be the Aerodynamic Design Point (ADP). The design specifications for the low-pressure and the high-pressure compressors assumed by GTlab [9][10], the in-house preliminary design software, are shown in Table 1. The GTlab (Gas Turbine Laboratory) program system is an interactive, cross-platform simulation and pre-design environment for aircraft engines and gas turbines. Specifications for other operating points such as the Top Of Climb (TOC) or the Cutback for example were also provided in this software.

	Low-pressure compressor	High-pressure compressor
Inlet Mass Flow	18.48 kg/s	18.48 kg/s
Pressure Ratio	2.38	12.24
Rotational speed	7613 rpm	17767 rpm

Table 1 - Design specifications for both compressors at the ADP assumed by GTlab

Based on the performance cycle of the engine a first estimate of the component's preliminary design was established using GTlab-Sketchpad, which provides quick calculation routines based on 1-D meanline algorithms, see Figure 1. This preliminary design has been used as a basis for the detailed design.

Three constraints for further the design of the compression system were introduced. The first condition was a maximal radius value at the tip of the Booster. The second one was a minimal radius

at the hub of HPC. Finally, a minimal height for the rotor blade rows of the last stage of the HPC was imposed.

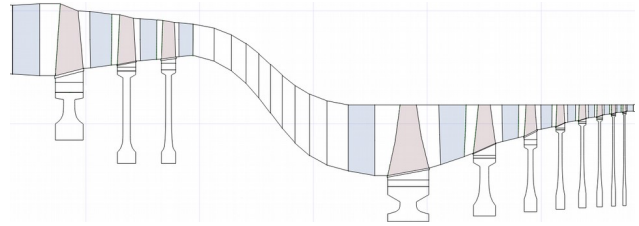


Figure 1 - Pre-design of the compression system used at the beginning of the study

## 2. DETAILED DESIGN

### 2.1. Booster and HPC Design

Throughflow calculations were performed with the in-house streamline curvature program "ACDC". This code was also used for studying compressor performance, checking important design parameters such as the De Haller number, the flow coefficient or the surge margin.

Regarding these preliminary design parameters, several conditions have been taken in account. The De Haller number was kept above 0.7 to reduce the viscous flow separation. The Lieblein's diffusion factor was kept less than 0.5 to ensure a wide operating range and provide high efficiency. The work coefficient was also kept below 0.5 to avoid overloaded blades. Regarding the distribution of the pressure ratio along the stages, a quite linear distribution has been selected. The number of the blades has also been taken into account for each blade row in order to decrease the weight of the compressor and adjusting the Lieblein's diffusion factor. Compared to the prediction made by GTlab, the number of blades has been slightly increased for the first stages of the high-pressure compressor and the Booster and highly decreased for the other stages. To obtain a more suitable aspect ratio for the blades, the length of the blades and also the axial length of the compressors have been modified. The axial length of the high pressure compressor has been reduced (48.5 cm instead of 50 cm) and the axial length of the Booster has been increased (38 cm instead of 32 cm). Only the first stage of the HPC has transonic rotor blade row. Concerning the tip clearance, the value of the rotor blades of each stage has been chosen in function of their blade height, regarding results provided by [2] and [6].

After the ICD design, modifications have been made to the last stage of the Booster by decreasing the radius, specially at the outlet of the OGV, in order to create a less aggressive design of the inter-compressor duct and to fulfill the design conditions of the inter-compressor duct.

The number of VGVs has also been chosen for each compressor to fulfill the surge margin at off-design speeds and also to reach the target conditions for all operating points from the specifications. Only the use of the IGV has been selected for the Booster. Concerning the HPC, three VGVs, including IGV, have been used, as well as a bleed after the second stage. The speedlines of the different operating points for the Booster and the HPC are illustrated Figure 2 and 3.

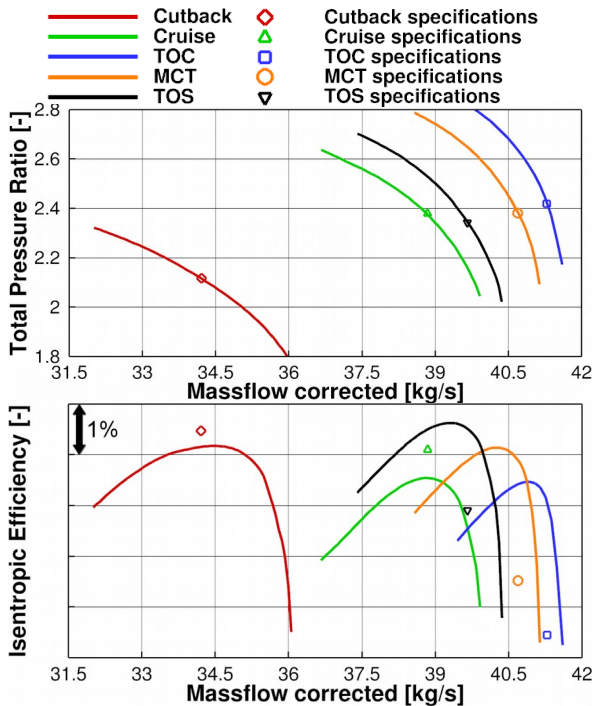


Figure 2 - Speedlines of the different operating points for the Booster

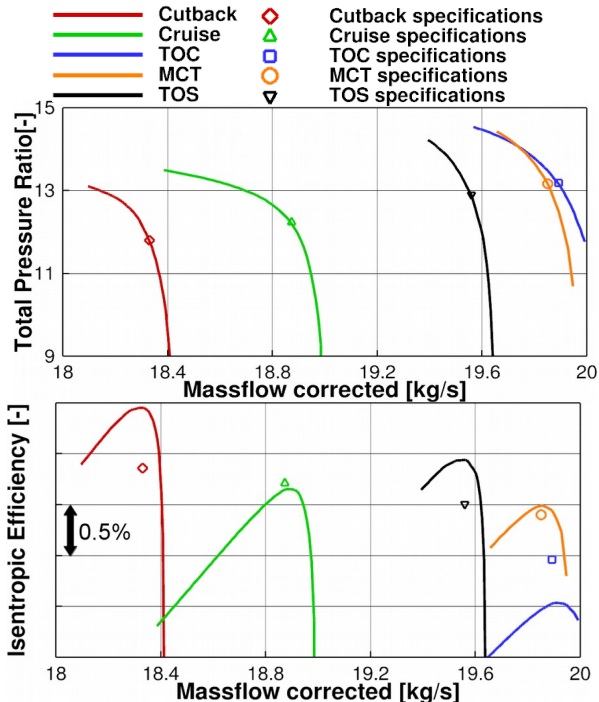


Figure 3 - Speedlines of the different operating points for the HPC

For an equivalent pressure ratio, the isentropic efficiency, obtained at the ADP for the Booster, is lower than assumed in the preliminary design. This is also the case for the isentropic efficiency of the HPC obtained at the ADP, which is slightly lower than assumed in the preliminary design.

Concerning the other operating points, better isentropic efficiency has been reached for the TOS, the MCT and the TOC of the low-pressure compressor, and for the Cutback the TOS and the MCT of the high-pressure compressor. But lower isentropic efficiency has been reached for the Cutback of the low-pressure compressor and for the TOC of the high-pressure compressor.

As it was explained before, throughflow calculations have been used to design the low-pressure compressor and the high-pressure compressor. However, after the check of 3D CFD results, modifications have been made at the hub of the first rotor of the high-pressure compressor in order to minimize the risk of flow separation.

## 2.2. ICD Design

After the design of the Booster and the HPC, the ICD has been designed.

3D CFD design has been used in the case of the ICD, due to the difficulties encountered to estimate the losses of the strut by throughflow calculations.

To achieve this design, the airfoil profile from [3] has been taken as a basis and a number of 8 struts has been chosen.

Additionally, main design parameters evoked in [4] have been checked, such as the duct turning angle  $\alpha$ , the ratio between the area at the inlet and at the outlet, and the ratio  $\frac{\Delta R}{L}$ .

The first design of the flowpath was realized without checking the main design parameters listed before.

For the second design, the axial length has been reduced in order to reduce the overall weight of the engine and to obtain a value closer to the typical values of the ratio  $\frac{\Delta R}{L}$ .

The profile of the strut has also been modified with a slight decrease of the maximal thickness. Concerning the duct turning angle, a value of  $48^\circ$  has been chosen and a typical value of 1 has been chosen for the area ratio between the inlet and the outlet of the ICD. Modifications have also been made on the Booster, as explained before, to fulfill the value of 1 for the area ratio. But the Mach number was too high in some regions of the ICD, specially at the inlet of the strut. The current design has been designed with a constant area along the ICD.

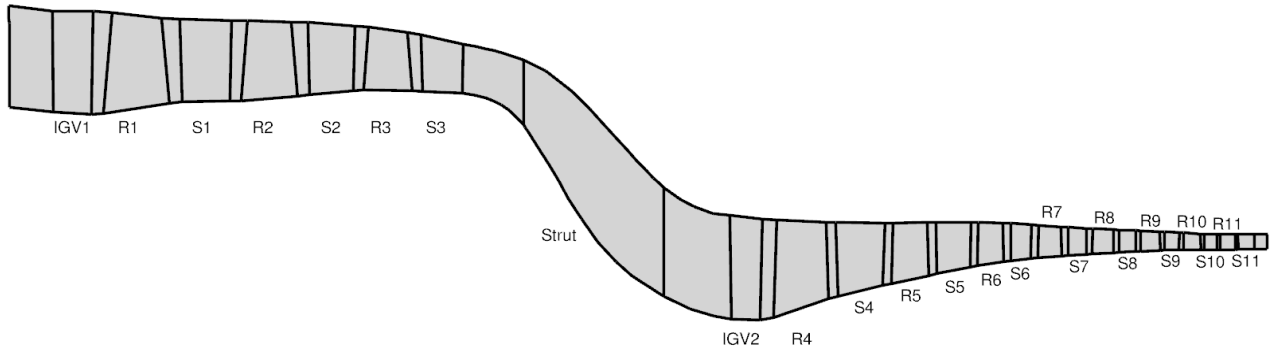


Figure 6 - Flowpath of the compression system

The strut has been moved as well and the strut profile has been modified by moving the position of the maximal thickness to avoid high Mach number values at the inlet. This last design provides typical Mach number values, with a peak at 0.65.

The evolution of the flowpath is shown in Figure 4, as well as the evolution of the profile in Figure 5. The current flowpath of the overall compression system is shown in Figure 6.

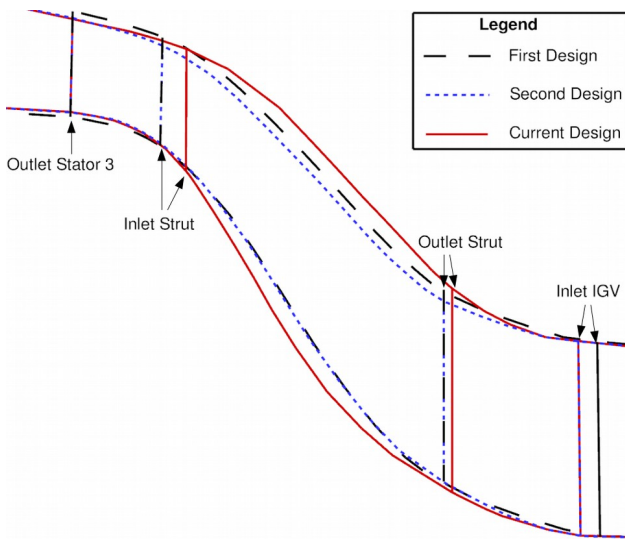


Figure 4 - Evolution of the flowpath of the ICD

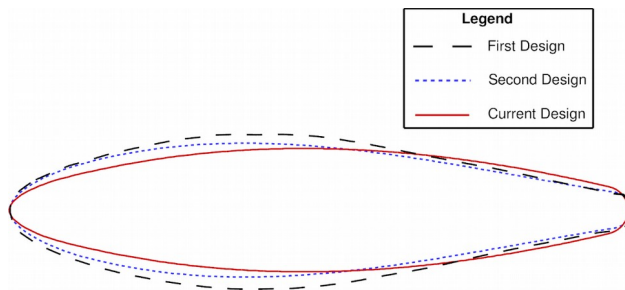


Figure 5 - Evolution of the profile of the Strut

## 2.3. Blading Design

The design of the blades has been realized with the use of a database of optimal airfoils [1] [5].

This database is composed of airfoils that have low losses and guarantee stable operation over wide incidence ranges. The airfoils, which composed this database, have been optimized by varying the following requirements : the inlet Mach number, the pitch-chord ratio, the stagger angle  $\gamma$ , the thickness-chord ratio, the diffusion factor, the Reynolds number and the MVDR.

During the optimization, five control points for the suction side and four control points for the pressure side have been used to define each airfoil and to assure a high degree of freedom, as it is shown in Figure 7. Furthermore, during the optimization of each airfoil, the performance at design and off design conditions have been evaluated with the blade-to-blade flow solver MISES.

Three optimized airfoils have been used to design each blade of the compression system : one at the hub, one at midspan, and one at the tip.

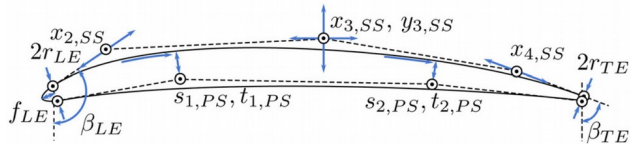


Figure 7 - Design parameters of airfoil geometry (Extracted from [5])

## 3. 3D CFD Validation

In order to validate the design realized with throughflow calculations, 3D CFD calculations have been made with "TRACE" [7] [8], an in-house 3D CFD code. Pre-processing has been realized with the software "GMC".

### 3.1. Grid generation

Each blade has been meshed with the in-house software PyMesh.

First, a 2D S2m grid has been generated. Eighty-five lines have been chosen for the radial direction, of which nine of them are in the tip clearance.

Then, a O-C-H grid has been chosen, and the

mesh generated for the hub and the tip of each blade. A refined mesh has been used, especially for the O-grid, in order to capture gradients, minimize numerical diffusion and because of the boundary layer. Each blade has been meshed separately and assembled with the software “GMC”. Approximately 1.2 million cells have been used for the mesh of each blade row.

### 3.2. Numerical setup

Steady computations were performed using 3D Navier-Stokes equations and the Wilcox k-w model was selected for the turbulence modeling. Two types of wall treatment have been used for this simulation. “Low Reynolds” wall treatment has been chosen for the blades surfaces, which means that the  $y^+$  value for these regions needed to be close to one. For the other surfaces, “Wall function” wall treatment has been selected, which means that the intended  $y^+$  value was above thirty. Bardina model have also been used to simulate rotational effects. No transition model was used for the simulations.

Concerning the boundary conditions, the six following parameters have been imposed at the computational domain entry: the absolute total pressure, the absolute total temperature, the turbulence intensity, the eddy length scale, the velocity angle  $R$ , and the absolute velocity angle  $\theta$ .

For the outlet conditions, a static pressure has been imposed. A mixing plane interface, which averages the flow quantities in the circumferential direction, has been used for the inlet and the outlet of each blade, except of course at the inlet of the IGV and the outlet of the OGV.

### 3.3. Booster simulation

The first 3D CFD calculations were conducted on the Booster. The goal of these simulations was to create the speedline around the ADP of the Booster with “TRACE” and to compare it with the speedline obtained with “ACDC”. The two speedlines are visualized in Figure 8.

Then, the ADP results obtained with ACDC have been compared with the results, obtained with “TRACE”, at an equivalent operating point.

The equivalent operating point has a pressure ratio of 2.35. The isentropic efficiency obtained with the 3D CFD code is 1% lower than the isentropic efficiency obtained with through-flow calculations. Averages values and radial distribution of the different parameters have been checked to know for which blade some differences were high. The Figure 9 shows the isentropic efficiency for each stage for “TRACE” and “ACDC” calculations.

As it can be seen, the main difference lies at the last stage where the isentropic efficiency obtained with “TRACE” calculations is 2% lower compared to

“ACDC” calculations, partly due to higher pressure losses than expected for the OGV of the Booster, specially at the hub and the tip of the blade, like it can be seen in Figure 10.

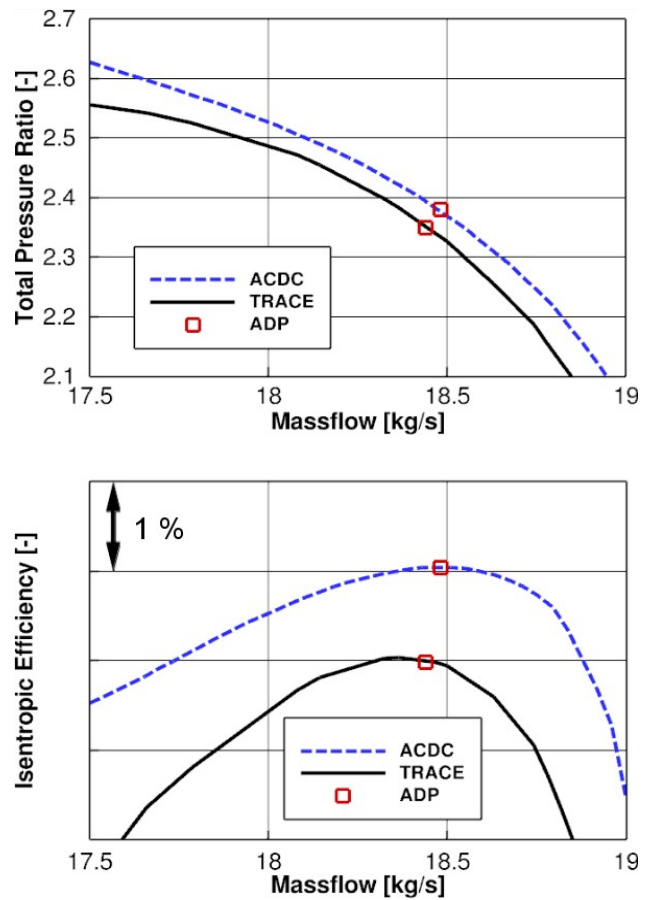


Figure 8 - Booster speedlines obtained with “TRACE” and “ACDC”

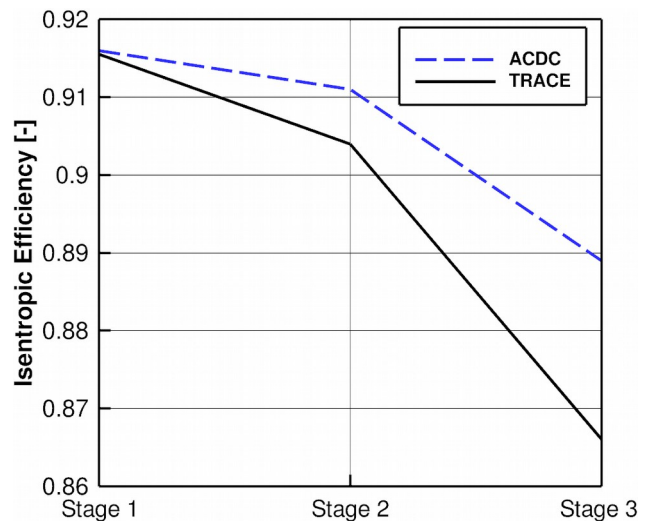


Figure 9 - Isentropic efficiency distribution along the stages of the Booster for “TRACE” and “ACDC” calculations

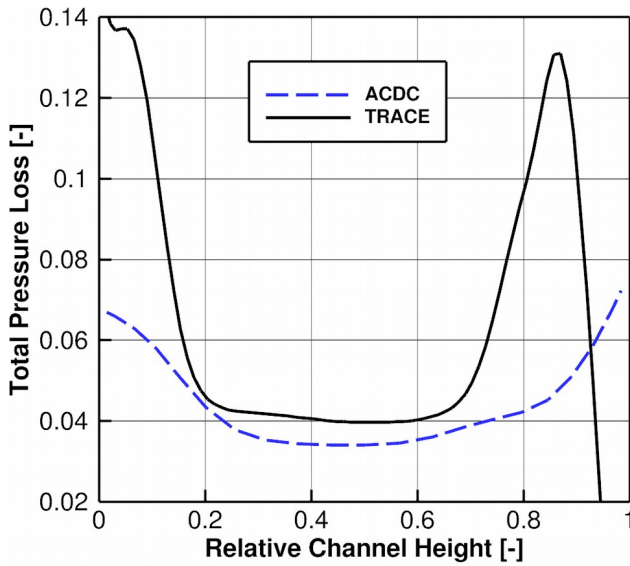


Figure 10 - Radial distribution of the total pressure loss of the OGV of the Booster

### 3.4. ICD simulation

After the 3D CFD calculations for the Booster, simulations have been conducted for the ICD to check for flow separations or regions with an high Mach numbers. Thanks to these simulations, modifications have been undertaken as it can be seen in Figure 4 and 5. The final design was validated, by the mean level of pressure losses of the strut and the Mach number distribution along the ICD. This distribution of the Mach number along the ICD is illustrated in Figure 11 and 12. High Mach number regions are located near the to high curvatures regions, and low Mach number regions are located near to the low curvatures regions.

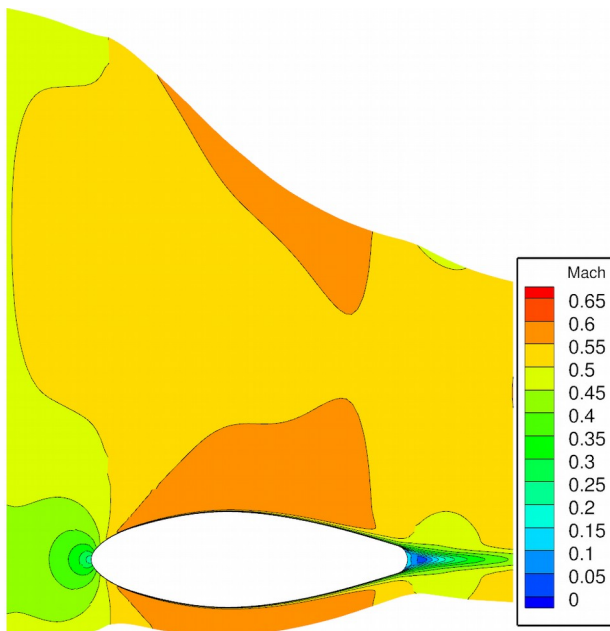


Figure 11 - Mach number distribution at midspan

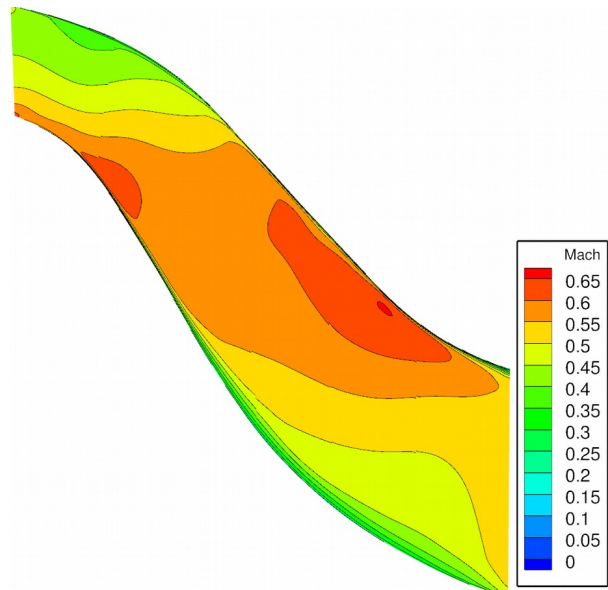


Figure 12 - Mach number distribution in S2m view

### 3.5. HPC simulation

3D CFD calculations, for the HPC, have only been conducted for the first two stages of the compressor. Like it was the case for the Booster, the speedline of the HPC has been computed to be compared with the “ACDC” speedline. The two speedlines are illustrated in Figure 13.

Then, the ADP results, obtained with ACDC, have been compared with the results, obtained with “TRACE”, of an equivalent operating point. The difference between the massflow of the operating point obtained on ACDC and TRACE was higher compared to the difference obtained for the Booster (1.8% for the HPC and 0.16% for the Booster).

The operating point equivalent to the ADP has a pressure ratio of 2.233, instead of 2.31 for “ACDC” Concerning the isentropic efficiency, a difference of 0.2% has been obtained between “ACDC” and “TRACE” results.

Concerning the pressure losses, which are visualized in Figure 14. The results obtained with the two methods are close, except for the IGV where the losses obtained with ACDC are underestimated.

### 3.6. Overall compression system simulation

After performing 3D CFD calculations for each main component of the compression system separately, new 3D CFD calculations have been conducted with the three parts linked together. The “TRACE” and “ACDC” speedlines have also been calculated in order to be compared and are shown in Figure 15.

A pressure ratio of 5.21 for the “TRACE” operating point has been reached compared to the pressure ratio of 5.45 for the “ACDC” operating point.

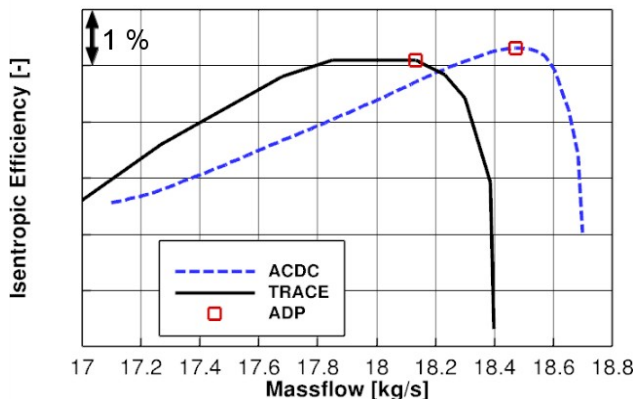
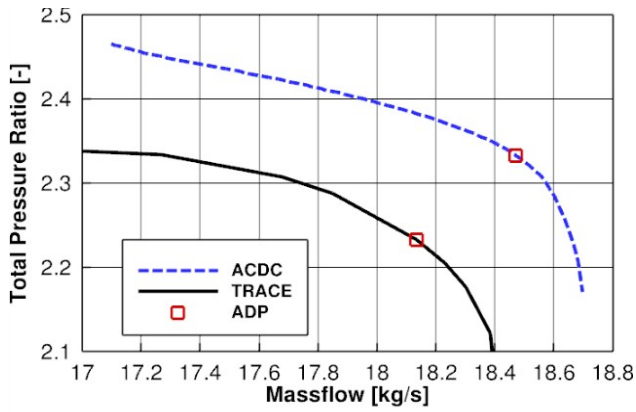


Figure 13 - HPC speedlines obtained with "TRACE" and "ACDC"

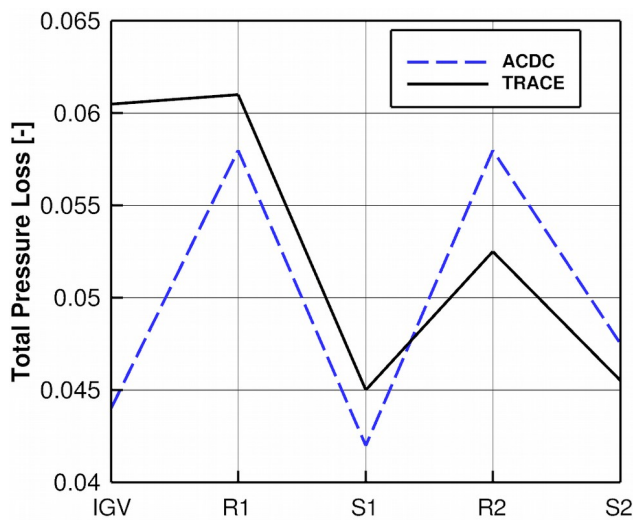


Figure 14 - Total pressure loss distribution along the blades of the first two stages HPC for "TRACE" and "ACDC" calculations

Concerning the isentropic efficiency, a difference of 1% between the two operating points has been observed. The difference between the massflow of the operating point obtained with "ACDC" and "TRACE" was 1.5%. The main difference observed, compared to the results obtained separately for each part of the compression system, was for the IGW of the HPC. Indeed, the pressure losses obtained for this blade was for this simulation to 0.08 instead of

0.06 for the simulation of the HPC only. This difference of results, when each part is simulated separately and the full system, can be explained by multiple reasons. The first reason is the cumulation of small differences in terms of flow angle or Mach number values for example, that can affect the following blades and so on. An other explanation would be the mixing losses at the several mixing planes when the full system is simulated. Concerning the results obtained for the other blades, averages values and radial distribution of the different parameters are generally close between "ACDC" and "TRACE". An example of the comparison is depicted in Figure 16, showing the radial distribution of the relative Mach number and relative whirl angle at the inlet of the first rotor of the Booster.

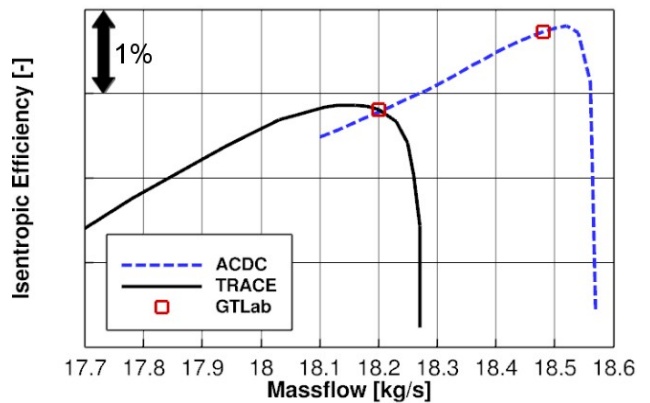
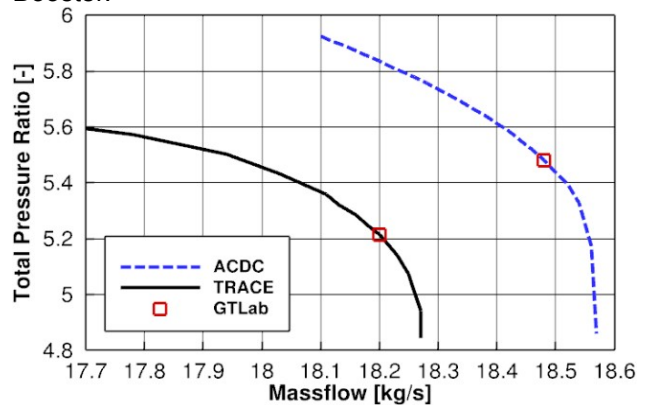


Figure 15 - Compression system speedlines obtained with "TRACE" and "ACDC"

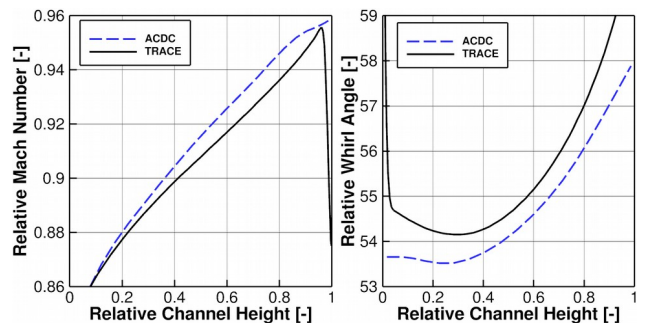


Figure 16 - Radial distribution of the relative Mach number and relative whirl angle at the inlet of the first rotor of the Booster

## CONCLUSION

A compression system, composed of the low-pressure compressor, the inter-compressor duct and the high-pressure compressor has been designed with throughflow calculations and validated with 3D CFD calculations. Each part of the compression system has been designed separately with the use of modern design methods.

Throughflow calculations provided results very close to the results obtained with 3D CFD calculations, when each part of the compressor has been simulated separately. Some differences appeared when the whole compression system was simulated, specially at the IGV of the high pressure compressor. However, the results obtained with throughflow calculations are still satisfactory compared to those obtained with 3D CFD calculations. Design improvements can be made, by iteratively computing 3D design for the full compressor. 3D CFD calculations on the full compression system, including the other stages of the high-pressure compressor can be conducted as well.

## REFERENCES

- [1] Schnoes, M. and Nicke, E. (2017), "Exploring a database of optimal airfoils for axial compressor design", in 'ISABE 2017', number ISABE-2017-21493, Manchester, England
- [2] Mileshin, V., Braiko, I., and Startsev, A., "Application of Casing Circumferential Grooves to Counteract the Influence of Tip Clearance", ASME, GT2008-51147, 1-11, Berlin, Germany, 2008
- [3] Donghai, J., Xiwu, L., Weiguang, Z., and Xingmin, G., Optimization of Endwall Contouring in Axial Compressor S-shaped ducts , CSAA, China, 1076-1086, 2015
- [4] Ortiz Dueñas, C., R. J. Miller, R. J., H. P. Hodson, H. P., and Longley, J. P., "Effect of Length on Compressor Inter-stage Duct Performance", ASME, GT2007-27752, 1-11, Montreal, Canada, 2007
- [5] Schnoes, M. and Nicke, E. (2017), 'A Database of Optimal Airfoils for Axial Compressor Throughflow Design', ASME J. Turbomach 139 (5), 051008.
- [6] Goto, A., Three-Dimensional Flow and Mixing in an Axial Flow Compressor with Different Rotor Tip Clearances, ASME paper, 91-GT-89, 1-11, Orlando, Florida, USA, 1991
- [7] Kügeler, E., Weber, A., Nürnberger, D., and Engel, K., 2008, "Influence of Blade Fillets on the Performance of a 15 Stage Gas Turbine Compressor", ASME Paper No. GT2008-50748, Berlin, Germany, 2008
- [8] Becker, K., and Kügeler, E., 2010, "Recent Progress in a Hybrid-Grid CFD Solver for Turbomachinery Flows", ECCOMAS CFD 2010, Lisbon, Portugal, June 14-17
- [9] Becker, R.-G., Reitenbach, S., Klein, C., Otten, T., Nauroz, M., "An integrated method for propulsion system conceptual design", ASME paper, GT2015-43251, Houston, Texas, USA, 2015
- [10] Becker, R.-G., Wolters, F., Nauroz, M., Otten, T., "Development of a Gas Turbine Performance Code and its Application to Preliminary Engine Design", DLRK paper, Bremen, Germany, 2011
- [11] Schnoes, M., and Voß, C., and Nicke, E., (2018) "Design Optimization of a Multi-Stage Axial Compressor Using Throughflow and a Database of Optimal Airfoils". In: Proceedings of the GPPS 2018. GPPS 2018, 7.-9. Mai 2018, Montreal, Canada.
- [12] Belamri, T., Galpin, P., Braune, A., Cornelius, C., "CFD Analysis of a 15 Stage Axial Compressor Part I: Methods", ASME, GT2005-68261, 1-8, Orlando, Florida, USA, 2005
- [13] Belamri, T., Galpin, P., Braune, A., Cornelius, C., "CFD Analysis of a 15 Stage Axial Compressor Part II: Results", ASME, GT2005-68262, 1-9, Orlando, Florida, USA, 2005
- [14] Steinke, R. J., "Design of 9.271 Pressure Ratio Five Stage Core Compressor and Overall Performance for First Three Stages", NASA Technical paper 2597, 1-35, Cleveland, Ohio, USA, May 1986
- [15] Sehra, A., Bettner, J., Cohn, A., "Design of a High Performance Axial Compressor for Utility Gas Turbine", ASME paper, 91-GT-145, 1-11, Orlando, Florida, USA, 1991
- [16] Küsters, B., Schreiber, H. A., Köller, U., Mönig, R., "Development of Advanced Compressor Airfoils For Heavy-Duty Gas Turbines Part 1: Experimental and theoretical analysis", ASME paper, Vol. 122, 406-415, Lake Alfred, Florida, USA 2000
- [17] Köller, U., Mönig, R., Küsters, B., Schreiber, H. A., "Development of Advanced Compressor Airfoils For Heavy-Duty Gas Turbines Part 1: Design and Optimization", ASME paper, Vol. 122, 397-405, Lake Alfred, Florida, USA, 2000

- [18] Gallimore, S. J., "Axial Compressor Design", ASME, GT2012-68524, 1-10, Copenhagen, Cambridge Turbomachinery Course, Cambridge University Whittle Laboratory, 2008, Denmark, 2012
- [19] Ikeguchi, T., Matsuoka, A., Sakai, Y., Sakano, Y., and Yoshiura, K., "Design and Development of a 14-Stage Axial Compressor for Industrial Gas Turbine", ASME, 2001-GT-0351, 1-8, New Orleans, Louisiana, 2001
- [20] Wellborn, S. R., and Delaney, R. A., "Redesign of a 12-stage axial flow compressor using multistage CFD", ASME, 2001-GT-0351, 1-8, New Orleans, Louisiana, 2001